Electrostatic potential in manganite-based heterojunctions by electron holography

H. F. Tian, J. R. Sun, H. B. Lü, K. J. Jin, H. X. Yang, H. C. Yu, and J. Q. Li[a)]
Beijing National Laboratory for Condensed Matter Physics, Institute of Physics, Chinese Academy of Sciences, Beijing 100080, People's Republic of China

(Received 4 January 2005; accepted 12 August 2005; published online 13 October 2005)

Electric potentials at the manganite-based heterojunctions, composed of $La_{0.9}Sr_{0.1}MnO_3$ and 0.01 wt % Nb-doped $SrTiO_3$ (*p-n* junction) and $La_{0.7}Ce_{0.3}MnO_3$ and 0.5 wt % Nb-doped $SrTiO_3$ (*n-n* junction), have been studied by means of off-axis electron holography. The experimental measurements demonstrate that evident electron diffusion from the *n*-type $SrNb_xTi_{1-x}O_3$ to the manganite films occurs in both *p-n* and *n-n* heterojunctions. The *p-n* heterojunction shows a complex potential change across the interface due to the variation of dielectric constant and electronic structure. *In situ* cooling experimental measurement on *n-n* junctions reveals an apparent change of potential along with the ferromagnetic phase transition. © *2005 American Institute of Physics*. [DOI: 10.1063/1.2084344]

Understanding of the energy barrier and charge diffusion in heterojunctions and the related semiconducting devices is one of the crucial issues in both academic research and technological applications. Artificial devices composed of the manganese oxides have been fabricated and analyzed following the discovery of remarkable physical properties in this strongly correlated system, such as the colossal magnetoresistance (CMR) and electronic phase separation.[1,2] Much experimental evidence on the artificially designed structures has verified new device concepts of the Schottky junction,[3,4] the field-effect transistor[5,6] and the *p-n* junction.[7–10] Our recent works suggest that the combination of the doped manganese oxides with other perovskite semiconductors is an effective way for fabricating junctions that show up notable magnetically tunable properties.

Recently, the electron holography technique becomes a powerful method for visualizing electromagnetic microfields in a variety of devices and yields both the one-dimensional and two-dimensional electric potential maps in typical systems.[11,12] In this letter two heterojunctions with different carrier concentrations,[13] composed of $La_{0.9}Sr_{0.1}MnO_3$ and 0.01 wt % Nb-doped $SrTiO_3$ (*p-n* junction) and $La_{0.7}Ce_{0.3}MnO_3$ and 0.5 wt % Nb-doped $SrTiO_3$ (*n-n* junction), have been investigated and analyzed in detail.

The *p-n* heterojunction was fabricated by growing a *p*-type $La_{0.9}Sr_{0.1}MnO_3$ (LSMO) film on *n*-type $SrTiO_3$ doped by 0.01 wt % Nb (SNTO1) using the laser molecular beam epitaxy. Electron microscopy and off-axis electron holography observations were carried out utilizing a Philips CM200/FEG transmission electron microscope equipped with the electrostatic biprism. Samples for cross-section TEM and electron holography investigations were prepared using a standard procedure consisting of gluing, cutting, mechanical polishing, dimpling, and ion milling.

Figure 1(a) is a bright-field TEM image displaying the cross-section morphology of the as-grown film with a uniform thickness of about 250 nm. The LSMO film shows a columnar structure originated from the interface to the film surface. The insets show the corresponding selected area electron diffraction pattern and high-resolution TEM image illustrating epitaxial relationship between LSMO film and the SNTO1 substrate. Systematical TEM investigations indicate that, in general, the LSMO films grow coherently on the substrate without notable mismatch dislocations; interfaces are clean and sharp without reaction products between the film and substrate.

Figure 1(b) shows a hologram taken at the interface region (indicated by arrows) under a positive biprism voltage of 90 V. This hologram is taken slightly off the zone axis direction for reducing dynamic effects. The interference

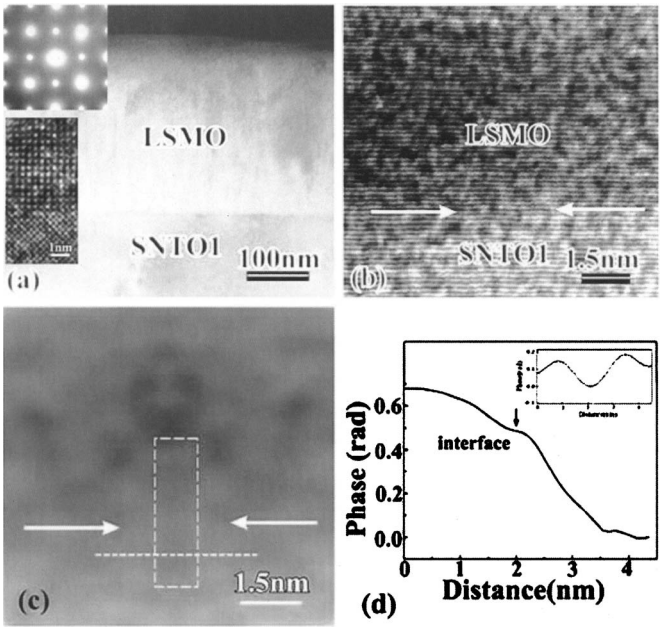

FIG. 1. (a) Bright-field TEM image showing morphology of the epitaxial LSMO film on SNTO1 substrate; the inset shows an electron diffraction pattern and the high-resolution TEM image from the interface area. (b) Hologram taken at 300 K for the interface area. Interface is indicated by arrows. (c) Reconstructed phase image from the hologram. Scanning is performed along the rectangular area. (d) Phase profile showing the phase change across the LSMO/SNTO1 *p-n* junction and inset is the phase profile parallel to the interface showing the noise fluctuation.

[a)]Author to whom correspondence should be addressed; electronic mail: ljq@aphy.iphy.ac.cn

fringes with perfect visibility have an average space of ~0.16 nm, therefore, the spatial resolution in the reconstructed holograms, about three times the fringe spacing, is better than 0.5 nm.[14] Figure 1(c) shows the typical area of the reconstructed phase image from Fig. 1(b), The averaged line scan from 30 pixels parallel to the interface [the rectangular area shown in Fig. 1(c)] gives a visible alternation across the junction. Figure 1(d) illustrates the typical phase modification normalized by the sample thickness. This averaged line profile is qualitatively in agreement with the theoretical expectation for the *p-n* heterojunction as discussed in the following context. The inset of Fig. 1(d) is the average phase profile parallel to the interface, in which the noise fluctuations are demonstrated with a magnitude of around 0.1 rad.

The phase changes on the junction are directly in connection with the potential barrier and charge distribution. Under experimental conditions with minimal dynamical diffraction effects, the phase shift of the object wave is given by

$$\varphi = C_E[V_0 t + V_{pn}(t - 2t_0)], \tag{1}$$

where C_E is a constant [$C_E = 7.295 \times 10^{-3}$ rad/(V nm) for 200 KeV electron], t is the sample thickness, and t_0 is the thickness of dead layer on each sample surface, it is mainly induced during the TEM sample preparation. The first term in the above equation arises from the mean inner potential V_0 of specimen.[15] We measured V_0 in $La_{1-x}Sr_xMnO_3$, $La_{1-x}Ce_xMnO_3$ and $Sr(Nb)TiO_3$, and we gave the mean inner potentials about 7.6 ± 1.3 V for $La_{1-x}Sr_xMnO_3$ and $La_{1-x}Ce_xMnO_3$ films and about 7 ± 0.9 V for the $Sr(Nb)TiO_3$ substrate. In our following analyses, this difference is systematically subtracted. The second term in Eq. (1) is produced by the local electrostatic potential V_{pn} for the *p-n* junction with which we are concerned chiefly in present study and can be written as

$$\varphi_{pn} = C_E V_{pn}(t - 2t_0). \tag{2}$$

For the present *p-n* (LSMO/SNTO1) heterojunction, the sample thickness t in the examined area was calculated from low loss electron energy-loss spectra using a method described by Egerton in Ref. 16 and confirmed by convergent beam electron diffraction. The measurements gave a value for $t \approx 50$ nm, and the experimental error is expected to be less then 10%. The thickness of the dead layer (t_0), shown up as amorphous layer, is found to be between 1 and 2 nm as observed by high-resolution TEM. We therefore can directly map the two-dimensional electrostatic potential for this *p-n* junction as $V_{pn} = \varphi_{pn}/50C_E$, which shows up a similar feature with the reconstructed phase map as shown in Fig. 1(d).

The heterojunction, in sharp contrast with the conventional *p-n* junction, has complex charge distribution and discontinuous electric fields due to the difference of dielectric constant between LSMO film and SNTO substrate. Figure 2(a) shows a line profile of the measured potential across the junction with subtracting the inner potential difference between film and substrate. The potential curve can be well interpreted by two potential functions written as

$$V_1 = \frac{qN_A(x_1 - x)^2}{2\varepsilon_1} \quad x_0 < x < x_1, \tag{3}$$

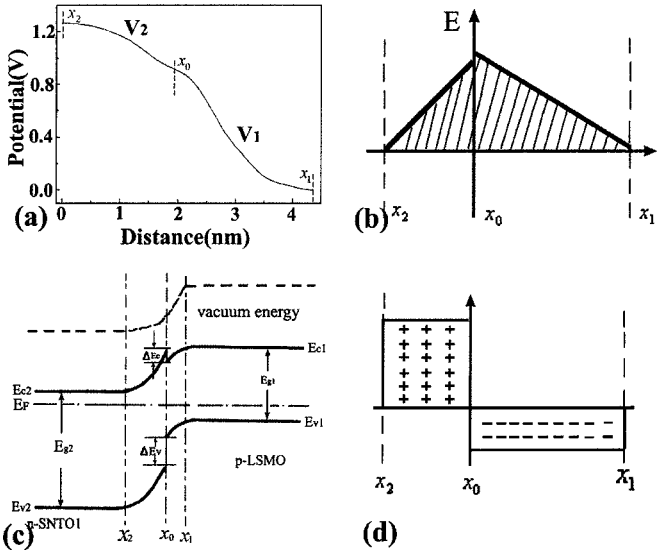

FIG. 2. (a) Averaged line profile showing the potential change of LSMO/SNTO1 *p-n* junction. (b) Electric field distribution across the junction. (c) Schematic of energy barrier across the *p-n* heterojunctions, the discontinuity of electronic bands is illustrated. The energy gap Eg_2 is ~3 eV for SNTO1 and the energy gap Eg_1 is ~1 eV for LSMO (see Ref. 6). (d) Charge distribution across the junction.

$$V_2 = V_D - \frac{qN_D(x - x_2)^2}{2\varepsilon_2} \quad x_2 < x < x_0, \tag{4}$$

where q is the electric charge, N_A is the acceptor impurity concentration in *p*-type region (LSMO film), N_D is the doped impurity concentration in *n*-type region (SNTO1 substrate), x_1, and x_2 is the width of the positive and negative space charge, and $\varepsilon_1, \varepsilon_2$ are, respectively, the dielectric constants of the substrate and film; x_0 is the interface position. These measurements give a clear potential of about 1.9 V at this *p-n* junction. Moreover, the electric field at this junction can be obtained from the derivative of the potential taken along the normal direction to the interface of the V_1 and V_2. We can obtain $E_1 = qN_A(x_1 - x)/\varepsilon_1$ and $E_2 = qN_D(x - x_2)/\varepsilon_2$. It is worth noting that an evident discontinuity occurs at the interface position ($\varepsilon_2 E_2 = \varepsilon_1 E_1$) as schematically illustrated in Fig. 2(b).

Actually, when the heterojunction consists of two different semiconducting materials, due to the difference in the dielectric constants, the band gaps, and the Fermi energy levels, energy band in general is discontinuous at the interface,[17] and a peak and a vale appear in the conducting energy band. Figure 2(c) illustrates schematically the energy band structure of the LSMO/STNO1 *p-n* junction. The band curves in the interface vicinity arise from the presence of electron potential. The scales of the peak and the vale on the conducting band depend mainly on interfacial charges on the junction. Eventually, the charge distribution nearby the junction can be obtained via the Poisson equation based on the potential of Fig. 2(b); Figure 2(d) shows a simplified illustration demonstrating the positive charges in $Sr(Nb)TiO_3$ and negative charges in the $La(Sr)MnO_3$ film.

To get a thorough understanding of the properties of the manganite-based heterojunction, an electron holography study was also performed for a nominal *n-n* heterojunction composed of an *n*-type $La_{0.7}Ce_{0.3}MnO_3$ (LCMO) film on a 0.5 wt % Nb-doped $SrTiO_3$ (SNTO2) substrate. The high-resolution TEM image in Fig. 3(a) demonstrates the epitaxial

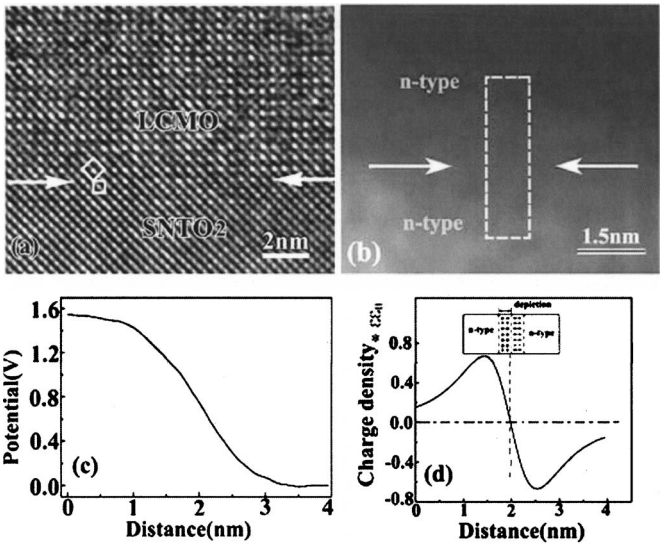

FIG. 3. (a) High-resolution TEM image of LCMO film on SNTO2 substrate. (b) Reconstructed phase image from the hologram. Scanning is performed along the rectangular area. (c) Phase profile showing potential change across the LCMO/SNTO2 *n-n* junction at 300 K. (d) Charge density at 300 K for the interface of LCMO/SNTO2 *n-n* junction. The inset shows the schematic space charge distribution of *n-n* junction structure.

growth of LCMO film and the perfect lattice coherence on the LCMO/STON2 interface. Figure 3(b) is a reconstructed phase image from an electron hologram taken under a positive biprism voltage of 90 V. A junction is visible in this phase image which clearly exhibits a noticeable contrast reversal between the LCMO film and SNTO2 substrate. An average line scan over 30 pixels [rectangular area in Fig. 3(b)] from the substrate to the film shows a remarkable potential change across the junction [Fig. 3(c)]. These data were normalized by film thickness which is measured to be ~55 nm on average and assumed to be constant within a few nanometers over the junction and with subtracting the inner potential difference between film and substrate. According to semiconducting theory, the depletion layer in an *n-n* junction is formed on the side with a larger band gap due to electron diffusion, i.e., the SNTO2 substrate in our case. In contrast, the charge layer on the opposite side (LCMO) may have an electron accumulation without charge depletion layer. Based on the variation of the potential, we can directly obtain the charge distribution across the junction as illustrated in Fig. 3(d). These results fundamentally agree with the standard model of heterojunction as illustrated in the inset of Fig. 3(d), and prove unambiguously a diffusion of electron from SNTO2 to LCMO.[9]

Another remarkable property observed in our experiments is the influence of the ferromagnetic (FM) transition of $La_{0.7}Ce_{0.3}MnO_3$ on the behavior of *n-n* heterojunction. The switch from the semiconducting to the metallic behavior, as demonstrated in the resistance-temperature curve in Fig. 4(a), occurs at the FM transition with critical temperature of ~300 K. *In situ* cooling electron holographic observations were performed from room temperature down to 120 K. Figure 4(b), from the same area of Fig. 3(c), shows the averaged potential distribution across the *n-n* heterojunction of LCMO/SNTO2 at 120 K. It is remarkable, in comparison with the data obtained at the room temperature, that the energy barrier becomes much higher and wider, i.e., the height

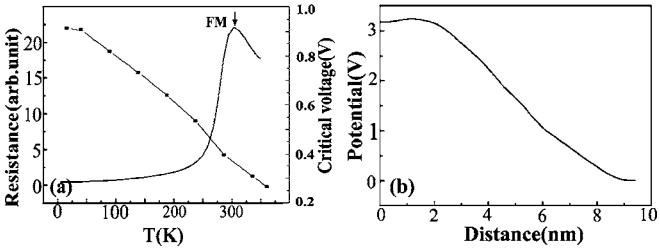

FIG. 4. (a) Temperature dependent resistance and critical voltage for LCMO film. (b) Potential change across the *n-n* junction as measured at 120 K.

rises from 1.57 V at 300 K to 3.1 V, and the width increases from 4 to 9 nm.

Generally, the relevant critical voltage is in correlation with a number of factors, but it is chiefly determined by the junction width and electrostatic potential. Hence, we can characterize the diffusion potential by the critical voltage corresponding to the rapid current increase in the *I-V* curves. Figure 4(c) shows the critical voltage as a function of temperature, clearly demonstrating the enhancement of the diffusion potential due to the FM transition. A visible kink appears in the critical voltage-temperature curve corresponding to the FM transition of LCMO. A rough estimation indicates the interfacial critical voltage is nearly doubled from 300 to 120 K; this change is qualitatively in agreement with the measured junction potential from electron holographic observations.

In summary, the experimental results demonstrate that evident electron diffusion from the *n*-type $SrTiO_3$ to the manganite films occurs in both *p-n* and *n-n* junctions.

The authors would like to thank Professor Y. Q. Zhou, Professor X. F. Duan, and Y. Li for their assistance in preparing samples. The work reported here was supported by the National Natural Science Foundation of China.

[1]G. V. Tendeloo, O. I. Lebedev, and S. Amelinckx, J. Magn. Magn. Mater. **211**, 73 (2000).
[2]A. Moreo, S. Yunoki, and E. Dagotto, Science **283**, 2034 (1999).
[3]T. Shimizu, N. Gotoh, N. Shinozaki, and H. Okushi, Appl. Surf. Sci. **117/118**, 400 (1997).
[4]T. Shimizu and H. Okushi, J. Appl. Phys. **85**, 7244 (1999).
[5]D. M. Newns, J. A. Misewich, C. C. Tsuei, A. Gupta, B. A. Scott, and A. Schrott, Appl. Phys. Lett. **73**, 780 (1998).
[6]J. A. Misewich and A. G. Schrott, Appl. Phys. Lett. **76**, 3632 (2000).
[7]H. B. Lü, S. Y. Dai, Z. H. Chen, L. Yan, Y. L. Zhou, and G. Z. Yang, Chin. Sci. Bull. **48**, 1328 (2003).
[8]J. R. Sun, C. M. Xiong, T. Y. Zhao, S. Y. Zhang, Y. F. Chen, and B. G. Shen, Appl. Phys. Lett. **84**, 1528 (2004).
[9]J. R. Sun, C. H. Lai, and H. K. Wong, Appl. Phys. Lett. **85**, 37 (2004).
[10]C. Mitra, P. Raychaudhuri, G. Köbernik, K. Dörr, K.-H. Müller, L. Schultz, and R. Pinto, Appl. Phys. Lett. **79**, 2408 (2001).
[11]M. R. McCartney, M. A. Gribelyuk, J. Li, P. Ronsheim, J. S. McMurray, and D. J. Smith, Appl. Phys. Lett. **80**, 3213 (2002).
[12]M. A. Gribelyuk, M. R. McCartney, J. Li, C. S. Murthy, P. Ronsheim, B. Doris, J. S. McMurray, S. Hegde, and D. J. Smith, Phys. Rev. Lett. **89**, 025502 (2002).
[13]H. B. Lu, S. Y. Dai, Z. H. Chen, Y. L. Zhou, B. L. Cheng, K. J. Jin, L. F. Liu, and G. Z. Yang, Appl. Phys. Lett. **86**, 032502 (2005).
[14]M. Gajdardziska-Josifovska, A. H. Carim, E. Völkl, L. F. Allard, and D. C. Joy, *Introduction to Electron Holography* (Kluwer/Plenum, New York, 1999).
[15]M. Gajdardziska-Josifovska, M. R. McCartney, W. J. de Ruijter, D. J. Smith, J. K. Weiss, and J. M. Zuo, Ultramicroscopy **50**, 258 (1993).
[16]R. F. Egerton, *Electron Energy-Loss Spectroscopy in the Electron Microscope*, 2nd ed. (Plenum, New York, 1996).
[17]R. K. Purohit, *Semiconductor Heterojunctions* (Oxford, Pergamon, 1974).